Shoaling transformation of wave frequency-directional spectra

T. H. C. Herbers and Mark Orzech
Department of Oceanography, Naval Postgraduate School, Monterey, California, USA

Steve Elgar
Department of Applied Ocean Physics and Engineering, Woods Hole Oceanographic Institution, Woods Hole, Massachusetts, USA

R. T. Guza
Integrative Oceanography Division, Scripps Institution of Oceanography, La Jolla, California, USA

Received 15 January 2002; revised 3 July 2002; accepted 24 July 2002; published 21 January 2003.

[1] A Boussinesq model for the nonlinear transformation of the frequency-directional spectrum and bispectrum of surface gravity waves propagating over a gently sloping, alongshore uniform beach is compared with field and laboratory observations. Outside the surf zone the model predicts the observed spectral evolution, including energy transfers to harmonic components traveling in the direction of the dominant waves, and the cross-interactions of waves traveling in different directions that transfer energy to components with the vector sum wavenumber. The sea surface elevation skewness and asymmetry, third-order moments believed to be important for sediment transport, also are predicted well. Effects of surf zone wave breaking are incorporated with a heuristic frequency-dependent dissipation term in the spectral energy balance equation and an empirical relaxation of the bispectrum to Gaussian statistics. The associated coefficients are calibrated with observations that span a wide range of surf zone conditions. With calibrated coefficients, the model predicts observed surf zone frequency spectra well and surf zone skewness and asymmetry fairly well. The observed directional spectra inside the surf zone are broader than the predicted spectra, suggesting that neglected scattering effects associated with the random onset of wave breaking or with higher-order nonlinearity may be important. *INDEX TERMS:* 4560 Oceanography: Physical: Surface waves and tides (1255); 4546 Oceanography: Physical: Nearshore processes; 4263 Oceanography: General: Ocean prediction; 4255 Oceanography: General: Numerical modeling; *KEYWORDS:* ocean waves, wave spectra, beach, surf

Citation: Herbers, T. H. C., M. Orzech, S. Elgar, and R. T. Guza, Shoaling transformation of wave frequency-directional spectra, *J. Geophys. Res.*, *108*(C1), 3013, doi:10.1029/2001JC001304, 2003.

1. Introduction

[2] Models for the transformation of ocean surface waves across a beach are important to the prediction of nearshore circulation and sediment transport. In addition to the well-understood linear processes of shoaling and refraction, the wave transformation is affected by nonlinear interactions and wave breaking. Nonlinear interactions between triads of wave components with frequencies (ω) and cross- (k) and alongshore (l) wavenumbers satisfying

$$\omega_1 + \omega_2 + \omega_3 = 0, \tag{1a}$$

$$k_1 + k_2 + k_3 = \Delta, \tag{1b}$$

$$l_1 + l_2 + l_3 = 0, \tag{1c}$$

where each component obeys the linear gravity wave dispersion relation and the mismatch from resonance Δ is small, transfer energy from the incident wave components to higher (e.g., harmonic) and lower (e.g., infragravity) frequency components. These interactions not only broaden the frequency spectrum in shallow water, but also phase-couple the spectral components, causing the characteristic steepening and pitching forward of near-breaking wave crests [e.g., *Freilich and Guza*, 1984; *Elgar and Guza*, 1985]. This nonlinear evolution is described well by depth-integrated Boussinesq equations for weakly nonlinear, weakly dispersive waves in varying depth [*Peregrine*, 1967]. Alternative forms of Boussinesq-type equations have been derived to extend their application to deeper water [e.g., *Kaihatu and Kirby*, 1995] and stronger nonlinearity [e.g., *Wei et al.*, 1995]. Recently, fully nonlinear Boussinesq equations [*Wei et al.*, 1995] have been used to describe the detailed time evolution of waves and wave-driven currents on complex bathymetry [*Chen et al.*, 2000]. All the above

0148-0227/03/2001JC001304$09.00

models are deterministic. That is, for a given set of time-dependent boundary conditions, the model yields time series of fluid velocities and sea-surface elevation at shoreward locations. Although these time-domain Boussinesq models can be applied to two-dimensional beaches with arbitrary incident wave conditions, the computations are numerically expensive for large domains and require detailed boundary conditions that often are not available.

[3] Alternatively, the shoaling evolution of random waves on a beach can be predicted with stochastic models that solve evolution equations for statistically averaged spectral wave properties [e.g., *Agnon and Sheremet*, 1997; *Herbers and Burton*, 1997]. These models are numerically efficient and can be initialized at the offshore boundary with wave spectra obtained from routine directional wave measurements or regional wave model predictions. However, unlike deterministic models that solve (approximate) equations of motion without any assumptions about higher-order statistics, stochastic models require a statistical closure that may yield significant errors over long propagation distances and in regions of strong nonlinearity.

[4] Theories for nonlinear wave-wave interactions are rigorous, but surf zone wave breaking is not well understood and is modeled heuristically. *Schäffer et al.* [1993] include a turbulent surface roller in a time domain Boussinesq model that yields a realistic description of the evolution of wave profiles in the surf zone. Most models for the breaking of random waves are based on the analogy of individual wave crests with turbulent bores [*Battjes and Janssen*, 1978; *Thornton and Guza*, 1983]. Although these bore models yield robust estimates of bulk dissipation rates in the surf zone, the spectral characteristics of the energy losses are not specified, and somewhat arbitrary quasi-linear spectral forms of the dissipation function are used in Boussinesq models [*Mase and Kirby*, 1992; *Eldeberky and Battjes*, 1996]. Boussinesq model predictions of wave frequency spectra in the surf zone appear to be insensitive to the precise frequency dependence of the dissipation function, but predictions of wave skewness and asymmetry are considerably more accurate if dissipation is weighted toward high-frequency components of the spectrum [*Chen et al.*, 1997]. Estimates of nonlinear energy transfers in the surf zone based on bispectral analysis of near-bottom pressure fluctuations confirm the dominant role of triad interactions in the spectral energy balance [*Herbers et al.*, 2000]. The observed decay of the spectral peak is primarily the result of large nonlinear energy transfers to higher frequencies where the energy presumably is dissipated.

[5] Although many studies of the shoaling evolution of wave frequency spectra have been reported, the evolution of the wave directional spectrum has received less attention, despite its potential importance to the generation of a longshore currents and infragravity motions. Laboratory and field measurements of wave directional spectra outside the surf zone show the expected refraction of incident waves and energy transfers to harmonic components with propagation directions that are in qualitative agreement with the theoretical interaction rules (1) [*Freilich et al.*, 1990; *Elgar et al.*, 1993]. Field observations of wave transformation across the surf zone show that wave breaking does not affect mean propagation directions significantly, but causes an increase in directional spreading that is not understood [*Herbers et al.*, 1999].

[6] Here, a numerical implementation and field evaluation of a stochastic Boussinesq model for directionally spread waves propagating over an alongshore uniform beach [*Herbers and Burton*, 1997] are presented. The model, based on a third-order closure, consists of a coupled set of first-order evolution equations for the wave spectrum $E(\omega, l)$ and bispectrum $B(\omega_1, l_1, \omega_2, l_2)$. The two-dimensional spectrum $E(\omega, l)$ defines the energy density of component (ω, l), and the four-dimensional (complex) bispectrum $B(\omega_1, l_1, \omega_2, l_2)$ defines the average phase relationship of a triad (Equation (1)) consisting of components (ω_1, l_1), (ω_2, l_2), and $(-\omega_1 - \omega_2, -l_1, -l_2)$. A one-dimensional version of the model for normally incident, non-breaking waves was developed and field-tested by *Norheim et al.* [1998]. The predicted evolution of wave frequency spectra agreed well both with observations and with predictions of the deterministic Boussinesq model of *Freilich and Guza* [1984]. Here, a full two-dimensional implementation of the model for directionally spread waves is presented, including heuristic extensions to incorporate dissipation associated with wave breaking (following *Kaihatu and Kirby* [1995]) and a relaxation to Gaussian statistics in regions of strong nonlinearity [e.g., *Orszag*, 1970; *Holloway and Hendershott*, 1977].

[7] The model (section 2) is evaluated with data from two field experiments on an ocean beach near Duck, North Carolina (described in section 3) and from a laboratory simulation of waves observed on a beach near Santa Barbara, California. Model predictions of the evolution of wave frequency-directional spectra, skewness, and asymmetry are compared with observations of nonbreaking (section 4) and breaking (section 5) waves, followed by a summary (section 6).

2. Model Description

2.1. Evolution Equations

[8] Spectral evolution equations for directionally spread surface gravity waves propagating over an alongshore uniform beach [*Herbers and Burton*, 1997] are reviewed briefly and extended to include heuristic surf zone damping and relaxation terms. The sea-surface elevation $\eta(x, y, t)$ of surface gravity waves propagating over an alongshore uniform beach has the general Fourier representation

$$\eta(x, y, t) = \sum_{p=-\infty}^{\infty} \sum_{q=-\infty}^{\infty} A_{p,q}(x) \exp\left[i\left(l_q y - \omega_p t\right)\right], \qquad (2)$$

where $\omega_p = p\Delta\omega$ and $l_q = q\Delta l$ are the frequency and alongshore wavenumber (with $\Delta\omega$ and Δl the separation of adjacent bands), x and y are cross- and alongshore space coordinates, respectively, and t is time. The water depth $h(x)$ is assumed to vary slowly in the cross-shore direction, and wave reflection from shore is neglected. Introducing small parameters for nonlinearity $\varepsilon = a_0/h_0$, dispersion $\sigma = \kappa_0 h_0$, and the medium variation $\chi = \beta_0/(\kappa_0 h_0)$ (where a_0, κ_0, h_0, and β_0 are representative values of the wave amplitude, wavenumber magnitude, water depth, and bottom slope, respectively), and assuming that ε, σ^2, and χ are all of the

same order, the evolution equation for the Fourier amplitude $A_{p,q}$ accurate to $O(\varepsilon^2)$ is

$$\frac{dA_{p,q}}{dx} = \left\{ -\frac{1}{4h}\frac{dh}{dx} - \alpha G(\omega_p, l_q) + i\left[\frac{\omega_p}{(gh)^{1/2}} + \frac{h^{1/2}\omega_p^3}{6g^{3/2}} - \frac{(gh)^{1/2} l_q^2}{2\omega_p}\right]\right\} A_{p,q} - i\frac{3\omega_p}{4h^{3/2}g^{1/2}} \sum_{m=-\infty}^{\infty}\sum_{n=-\infty}^{\infty} A_{m,n}A_{p-m,q-n}, \quad (3)$$

where g is gravity, and a quasi-linear damping term has been added to account for energy losses in the surf zone. The damping coefficient α depends on local wave properties and G is a spectral weighting function.

[9] In the limit of $\Delta\omega$, $\Delta l \to 0$, a continuous spectrum and bispectrum can be defined as

$$E(\omega_p, l_q) = \lim_{\Delta\omega,\Delta l\to 0} \frac{\langle A_{p,q}A_{-p,-q}\rangle}{\Delta\omega\Delta l}, \quad (4a)$$

$$B(\omega_m, l_n, \omega_{p-m}, l_{q-n}) = \lim_{\Delta\omega,\Delta l\to 0} \frac{\langle A_{m,n}A_{p-m,q-n}A_{-p,-q}\rangle}{\Delta\omega^2\Delta l^2}, \quad (4b)$$

where $\langle\ \rangle$ indicates the expected value. The evolution equations for E and B are (see *Herbers and Burton* [1997] for details):

$$\frac{dE(\omega,l)}{dx} = \left\{-\frac{1}{2h}\frac{dh}{dx} - D_1(\omega,l)\right\}E(\omega,l) + \frac{3\omega}{2h^{3/2}g^{1/2}}\int_{-\infty}^{\infty} dl' \int_{-\infty}^{\infty} d\omega' IM\{B(\omega', l', \omega-\omega', l-l')\} \quad (5a)$$

$$\frac{dB(\omega', l', \omega-\omega', l-l')}{dx} = \left\{-\frac{3}{4h}\frac{dh}{dx} - D_2(\omega', l', \omega-\omega', l-l') - i\left[\frac{h^{1/2}\omega'(\omega-\omega')\omega}{2g^{3/2}} + \frac{(gh)^{1/2}(\omega l' - \omega' l)^2}{2\omega'(\omega-\omega')\omega}\right]\right\} \cdot B(\omega', l', \omega-\omega', l-l') - i\frac{3}{2h^{3/2}g^{1/2}}[\omega' E(\omega-\omega', l-l')E(\omega,l) + (\omega-\omega')E(\omega', l')E(\omega,l) - \omega E(\omega', l')E(\omega-\omega', l-l')] + C^4(\omega', l', \omega-\omega', l-l') \quad (5b)$$

where IM $\{\}$ indicates the imaginary part, the damping terms D_1 and D_2 are given by

$$D_1(\omega,l) = \alpha[G(\omega,l) + G(-\omega,-l)] \quad (6a)$$

$$D_2(\omega', l', \omega-\omega', l-l') = \alpha[G(\omega', l') + G(\omega-\omega', l-l') + G(-\omega,-l)] \quad (6b)$$

and the fourth-order cumulant C^4 contains integrals over the trispectrum.

[10] *Herbers and Burton* [1997] use the quasi-normal closure hypothesis $C^4 = 0$, which is consistent with steady solutions for second-order bound waves and accurately reproduces the observed evolution of frequency spectra of nonbreaking waves on a natural beach [*Norheim et al.*, 1998]. However, the quasi-normal closure approximation is not satisfactory for modeling wave evolution over large distances or through regions of strong nonlinearity and wave breaking, producing an unrealistic divergence from Gaussian statistics that leads to large spatial oscillations and negative values of spectral levels [e.g., *Orszag*, 1970]. Although the neglected higher-order cumulant terms are believed to remain small, they are important in maintaining near-Gaussian statistics. The closure of equation (5b) can be improved by replacing the approximation $C^4 = 0$ with a relaxation term $C^4 = -\beta B$, where the coefficient β defines the distance over which phase coupling is destroyed [e.g., *Holloway and Hendershott*, 1977 and references therein]. Here β was assumed also to be proportional to the damping coefficient D_2, yielding

$$C^4(\omega', l', \omega-\omega', l-l') = -RD_2(\omega', l', \omega-\omega', l-l')B(\omega', l', \omega-\omega', l-l'), \quad (7)$$

with a (nondimensional) proportionality factor R that will be determined empirically. For $R = O(1)$ the relaxation to Gaussian statistics occurs over distances comparable with the surf zone width. Outside the surf zone where D_1 and D_2 are negligible, C^4 also is small (compared with the nonlinear interaction terms), and thus the closure model retains the appropriate quasi-normal approximation [*Herbers and Burton*, 1997].

2.2. Parameterization of Surf Zone Dissipation

[11] Following *Kaihatu and Kirby* [1995] and *Chen et al.* [1997], wave energy losses in the surf zone are parameterized with a simple quasi-linear damping term (equations (3), (5), and (6)). The spectral weighting function $G(\omega, l)$ has a quadratic frequency dependence [*Mase and Kirby*, 1992] and is independent of the wave direction

$$G(\omega,l) = \omega^2 \quad (8)$$

Chen et al. [1997] show that the frequency dependence in equation (8) yields more accurate predictions of wave skewness and asymmetry in the surf zone than a uniform (frequency-independent) weighting. Although weighting the dissipation towards higher frequencies does not affect the spectral shape evolution significantly, it strongly enhances nonlinear energy transfers and phase coupling between the dominant swell and higher frequency components, qualitatively consistent with direct observations of the spectral energy balance in the surf zone [*Herbers et al.*, 2000]. No attempt was made to include a directional dependence in the spectral weighting function G because the effects of directional spreading on wave breaking and dissipation are not understood.

[12] Reliable estimates of the bulk dissipation rate (i.e., integrated over all spectral components) can be obtained with widely used random wave decay models based on the analogy with turbulent bores [*Battjes and Janssen*, 1978].

Each breaking wave in a random wave field is treated as a turbulent bore for which the dissipation rate is obtained as a function of the bore height from mass and momentum conservation arguments [*Lamb*, 1932]. The average dissipation rate per unit sea surface area is then evaluated by weighting the predicted energy losses in individual waves with a probability distribution of breaking wave heights. *Thornton and Guza* [1983] refined the *Battjes and Janssen* [1978] model by introducing a more realistic breaking wave height distribution based on field measurements. Including further empirical improvements [*Whitford*, 1988], the expression for the bulk average dissipation rate used here is

$$D = \frac{3\rho g b \gamma}{4\sqrt{\pi}} m_1 H_r \{1 + \tanh[8(H_r - 1)]\}\left\{1 - \left(1 + H_r^2\right)^{-5/2}\right\}. \tag{9}$$

The adjustable coefficient γ is a representative ratio between breaker height and water depth, and ρ is the density of sea water. The dissipation rate is reduced by a factor b because, unlike a fully developed bore, the turbulent front of a breaking wave typically covers only part of the wave crest. The spectral moments m_n are defined as

$$m_n = \int_{-\infty}^{\infty} dl \int_{-\infty}^{\infty} d\omega |\omega^n| E(\omega, l), \tag{10}$$

and $H_r \equiv 2\sqrt{2} m_0^{1/2}/\gamma h$ is the ratio between the root-mean-square average wave height and the breaker height.

[13] The damping coefficient α (equation (6)) follows from expressing the spectral energy balance (equation (5a)) in flux form and integrating over all frequencies and alongshore wavenumbers

$$\frac{d}{dx}\left(\rho g^{3/2} h^{1/2} m_0\right) = -2\rho g^{3/2} h^{1/2} \alpha m_2. \tag{11}$$

The integral of the nonlinear interaction term of equation (5a) vanishes because energy is conserved within each resonant triad [*Herbers and Burton*, 1997]. To leading order the left-hand side of equation (11) is the cross-shore divergence of the energy flux, and the right-hand side equals the net dissipation rate $-D$. Thus equating the right-hand side to equation (9) yields

$$\alpha = \frac{3b\gamma}{8\sqrt{\pi}\sqrt{gh}} \frac{m_1}{m_2} H_r \{1 + \tanh[8(H_r - 1)]\}\left\{1 - \left(1 + H_r^2\right)^{-5/2}\right\}. \tag{12}$$

[14] The full parameterization of surf zone effects, equations (6)–(8) and (12), contains three adjustable coefficients γ, b, and R. Optimal values $\gamma = 0.3$, $b = 0.25$, and $R = 2.5$ were determined by minimizing errors in model predictions of waves observed in the surf zone (Appendix A).

2.3. Numerical Implementation

[15] The evolution equations (5a, 5b) were discretized in finite frequency [0, ω_{max}] and alongshore wavenumber [$-l_{max}$, l_{max}] domains, utilizing symmetry relations to reduce the computational effort (Appendix B). A fourth-order Runge Kutta scheme with a fixed step size was used to integrate equations (5a) and (5b) simultaneously from the offshore boundary across the beach. Here, the spectra were described with 50 frequencies and 85 alongshore wavenumbers, giving a total of 3,386,875 triads (Appendix B). The maximum wave frequency f_{max}(= $\omega_{max}/2\pi$) was set to 0.34 Hz to resolve the dominant swell and several harmonics. The maximum alongshore wavenumber l_{max} was 0.19 rad/m, restricting the wave incidence angle at the highest frequency and shallowest array to ±23° (restrictions on the angle are less severe at lower frequencies and greater depths). The energy levels at high frequencies are relatively low and interactions involving waves propagating at large oblique angles are far from resonance [e.g., *Phillips*, 1960]. Thus these neglected components do not contribute significantly to the spectral evolution, although the associated rapid biphase variations tend to destabilize the numerical integration of equation (5b). A relatively small integration step size of 0.25 m was necessary to resolve the fastest biphase variations in the model. Further model developments to achieve greater numerical efficiency (e.g., larger step sizes and fewer triads) by removing interactions that are far from resonance will be presented elsewhere.

2.4. Boundary Conditions

[16] The model initialization requires a spectrum $E_0(\omega, l)$ and bispectrum $B_0(\omega_1, l_1, \omega_2, l_2)$ at the offshore boundary. In many applications an estimate of the frequency-directional spectrum $E_0(f, \theta)$ of incident waves can be obtained from the output of operational spectral wave prediction models [e.g., *WAMDI Group*, 1988] or from nearby wave measurement systems (e.g., pitch-and-roll buoys). In this study, high-resolution estimates of $E_0(f, \theta)$ were available from arrays of pressure sensors (described below). Applying the Jacobian transformation

$$E(\omega, l) = \frac{E(f, \theta)}{4\pi\kappa \cos(\theta)} \tag{13}$$

to $E_0(f, \theta)$, where the wavenumber κ is given by the linear dispersion relation $\omega^2 = g\kappa \tanh(\kappa h)$, yields the initial spectrum $E_0(\omega, l)$.

[17] To obtain stable estimates of the initial bispectrum $B_0(\omega_1, l_1, \omega_2, l_2)$ from field measurements requires an extensive alongshore array of sensors that usually is not available. Instead, B_0 is approximated with the steady, uniform depth solution to equations (5a) and (5b) (with D_1, D_2, and C^4 set equal to zero):

$$\begin{aligned} B_0(\omega_1, l_1, \omega_2, l_2) = &\left[\frac{h_0^2 \omega_1 \omega_2 (\omega_1 + \omega_2)}{3g} + \frac{g h_0^2 (\omega_1 l_2 - \omega_2 l_1)^2}{3\omega_1 \omega_2 (\omega_1 + \omega_2)}\right]^{-1} \\ &\cdot\{(\omega_1 + \omega_2) E_0(\omega_1, l_1) E_0(\omega_2, l_2) \\ &-\omega_1 E_0(\omega_2, l_2) E_0(\omega_1 + \omega_2, l_1 + l_2) \\ &-\omega_2 E_0(\omega_1, l_1) E_0(\omega_1 + \omega_2, l_1 + l_2)\}, \end{aligned} \tag{14}$$

where h_0 is the water depth at the offshore boundary. This closed-form solution of the evolution equations (discussed in more detail by *Herbers and Burton* [1997]) describes

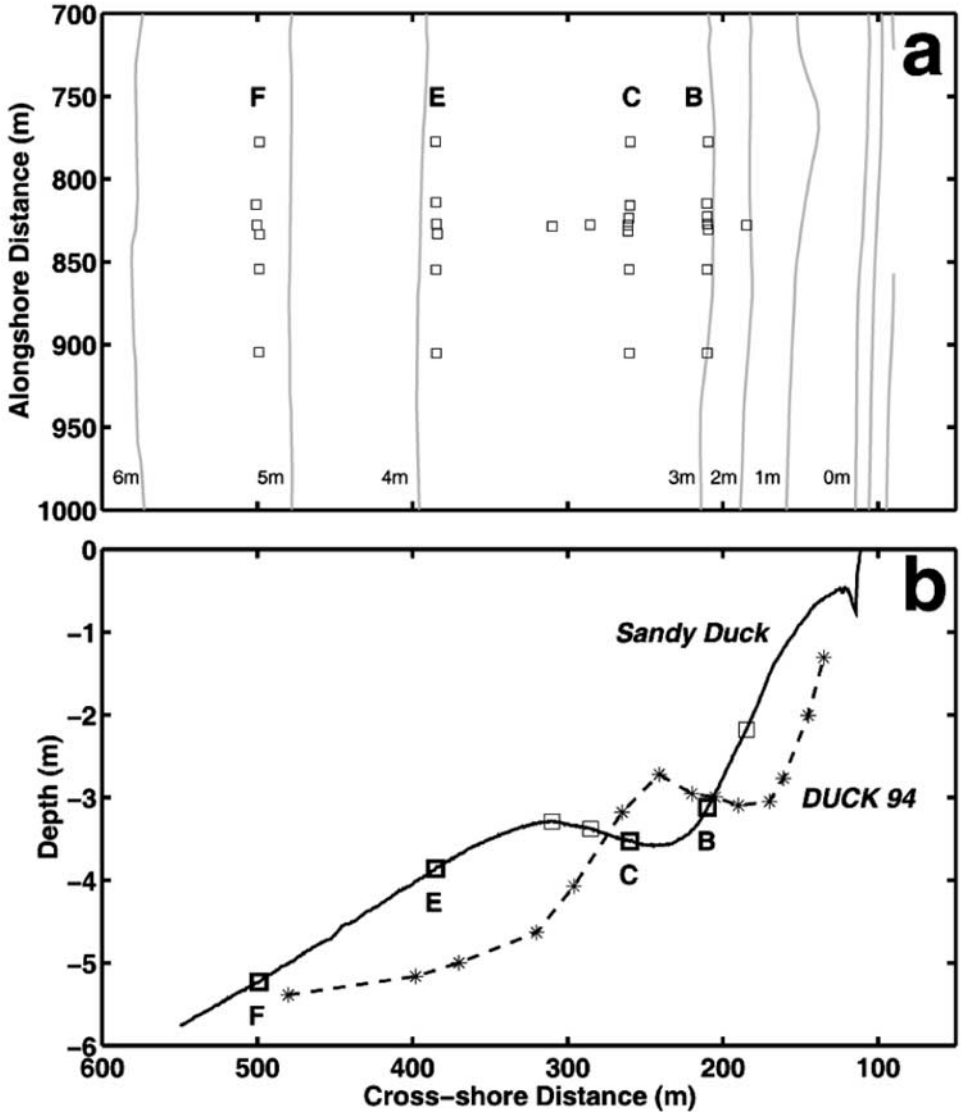

Figure 1. (a) Plan view of four alongshore arrays (labeled B, C, E, F) and a cross-shore transect of colocated pressure sensors and current meters deployed during SandyDuck. Instrument locations (squares) are given in the local beach coordinate system of the Field Research Facility. Solid curves are representative depth contours (relative to mean sea level). (b) Representative beach profiles along the instrumented cross-shore transects during SandyDuck (solid) and DUCK94 (dashed, each asterisk is a colocated pressure sensor and current meter).

skewed wave profiles with zero asymmetry (B_0 is real), in good agreement with local wave properties observed well outside the surf zone on a gently sloping seabed [e.g., *Herbers et al.*, 1992]. It is shown below (e.g., Figure 3) that B_0 provides an accurate offshore boundary condition for predicting the shoaling evolution to asymmetric wave profiles farther inshore.

3. Field Experiments and Data Analysis

[18] Detailed measurements of waves shoaling across an ocean beach were collected during the DUCK94 (Fall 1994) and SandyDuck (Fall 1997) experiments (Figure 1) at the U.S. Army Corps of Engineer's Field Research Facility (FRF) located near Duck, North Carolina. During DUCK94 a cross-shore transect of 14 pressure gauge-current meter pairs was deployed between the shoreline and about 5 m depth (Figure 1b) [*Elgar et al.*, 1997]. A downward-looking sonar altimeter colocated with each instrument pair provided continuous seafloor elevation measurements. Detailed incident wave directional properties were estimated with measurements from a linear alongshore array of pressure sensors (9 elements, 255 m aperture) maintained by the FRF in 8 m depth, about 800 m from shore. Data were collected nearly continuously at 2 Hz during September and October 1994. Conditions during the experiment are described by *Feddersen et al.* [1998].

[19] During SandyDuck a two-dimensional array of pressure gauges, current meters, and altimeters was deployed between the shoreline and 5 m depth (Figure 1) [*Elgar et al.*,

2001]. Four linear alongshore arrays of pressure sensors, each with 6–7 elements and an aperture of 127 m, were deployed to measure the evolution of the frequency-directional wave spectrum $E(f, \theta)$. These arrays (labeled B, C, E, and F in Figure 1a) were located about 96, 147, 271, and 385 m from the shoreline in nominal depths of 3.0, 3.6, 3.7, and 5.2 m, respectively. Three additional pressure sensors deployed along a cross-shore transect (Figure 1) were used to examine the cross-shore evolution of the wave field. Data were collected nearly continuously at 2 Hz between 2 August and 3 December 1997.

[20] Bathymetry surveys conducted by FRF staff using the Coastal Research Amphibious Buggy (CRAB) indicate that the beach was approximately alongshore uniform in both experiments. Alongshore homogeneity over the extent of the SandyDuck alongshore arrays was verified by comparing the measured energy density spectra from different sensors in each array, as well as by comparing coherence and phase spectra for redundant array lags. Instruments located farther south, close to the FRF pier, sometimes recorded anomalously low wave energy levels [*Elgar et al.*, 2001] and therefore were excluded.

[21] Beach profiles used in the model predictions for DUCK94 were obtained through linear interpolation of altimeter measurements. The cross-shore altimeter array in SandyDuck was sparse, and thus beach profiles used for SandyDuck predictions were estimated from a CRAB survey (usually collected within a few days to a week of the wave record). Tide corrections to the water depths were based on a tide gauge operated by the FRF in 8 m depth. During DUCK94 a well-developed sand bar (Figure 1b) was located approximately 100 m from shore until mid-October when it moved about 80 m farther offshore during a storm [*Gallagher et al.*, 1998]. At low tide, intense wave breaking and large energy losses often were observed across the shallow ($h \approx 2$ m) bar crest [*Elgar et al.*, 1997; *Herbers et al.*, 2000]. During SandyDuck the crest of the sand bar was located farther offshore and was more submerged (Figure 1b, $h \approx 3$ m at low tide), causing wave breaking on only a few occasions in extreme conditions.

[22] Wave frequency-directional spectra were estimated from the alongshore arrays of pressure sensors (8 m depth array in DUCK94, arrays F, E, C, B in SandyDuck, Figure 1a) for 3-hour-long data records with weak tidal sea level changes (<0.3 m) and approximately stationary wave conditions (changes in variance <15%). Cross-shore arrays were not used in these estimates because cross-shore depth changes cause significant variations in spectral levels, particularly in the surf zone where strong dissipation causes large gradients in wave height. The directional ambiguity of the linear arrays was resolved by neglecting weak reflection of waves from shore [*Elgar et al.*, 1994]. Array cross-spectra were calculated based on Fourier transforms of overlapping 1024-s segments. Merging seven frequency bands resulted in estimates with a frequency resolution of 0.0068 Hz and approximately 140 degrees of freedom. At each frequency f, the directional distribution of wave energy $S(\theta; f)$ was estimated from the array cross-spectra using a variational technique [*Herbers and Guza*, 1990]. The direction θ is defined relative to the local shoreline orientation, with $\theta = 0$ corresponding to normal incidence to the beach (waves arriving from 70° true N), and θ is positive (negative) for waves approaching the beach from northerly (southerly) directions. The surface elevation frequency spectrum $E(f)$ was obtained by applying a linear theory depth correction to the pressure auto-spectra and averaging the spectra of all sensors in the alongshore array. The $S(\theta; f)$ and $E(f)$ estimates were combined to form the wave frequency-directional spectrum $E(f, \theta) \equiv E(f)\, S(\theta; f)$. Additionally, $E(f)$ was estimated from all single pressure gauges in the cross-shore transects (Figure 1b).

[23] Bulk statistics of the wave field also were computed. The significant wave height H_s ($4\sqrt{E}$, with E the surface elevation variance) was estimated at each instrument site by integrating the surface elevation spectrum. The wave skewness and asymmetry moments, often used to describe the "peakedness" and degree of "pitching forward" of wave crests, were evaluated from the bottom pressure time series (see *Elgar and Guza* [1985] for definitions). Bulk mean wave directions $\bar{\theta}$ and directional spread σ_θ were estimated from current meter records (see *Herbers et al.* [1999] for details). The infragravity frequency range $f < 0.05$ Hz was excluded from all bulk wave statistics because the strong shoreline reflection of these low-frequency waves is not represented in the model.

4. Spectral Evolution Seaward of the Surf Zone

[24] For low to moderate waves the SandyDuck arrays (Figure 1a) were outside the surf zone. Wave breaking was confined primarily to the steep beach face inshore of the B-array, although occasional breaking of larger waves farther offshore resulted in some dissipation between the C- and B-arrays. In these conditions refraction and nonlinear triad interactions dominated the spectral evolution between the arrays, allowing for a quantitative verification of the representation of these conservative processes in the Boussinesq model. Observations are compared with model predictions for two representative case studies. In both cases the model was initialized with the observed frequency-directional spectrum $E(f, \theta)$ at the most offshore F-array and integrated for 300 m across the beach to the shallowest instrument (Figure 1).

[25] On 10 August the wave field observed at the F-array consisted of narrow band swell with a significant wave height $H_s = 0.9$ m, a peak frequency $f_p = 0.09$ Hz, and a mean direction (at f_p) close to normal incidence (−5°) (Figure 2). The model predicts the observed growth of harmonic peaks at frequencies $2f_p$ (resulting from energy exchanges in triads with frequencies of approximately f_p, f_p, and $2f_p$) and $3f_p$ (f_p, $2f_p$, $3f_p$ triads). The spectral levels of the predicted primary and harmonic peaks are in excellent agreement with the observations (Figure 2, upper panels). Observed and predicted harmonic spectral levels more than double between the F- and C-arrays, followed by a smaller decrease between the C- and B-arrays (and a corresponding increase in the primary peak level), indicating a reversal in nonlinear energy transfers over the trough in the seafloor profile inshore of the sand bar (Figure 1b), similar to earlier results at this site [*Norheim et al.*, 1998].

[26] The predicted evolution of directional wave properties also is in good agreement with the observations. In shallow water, where waves are weakly dispersive and

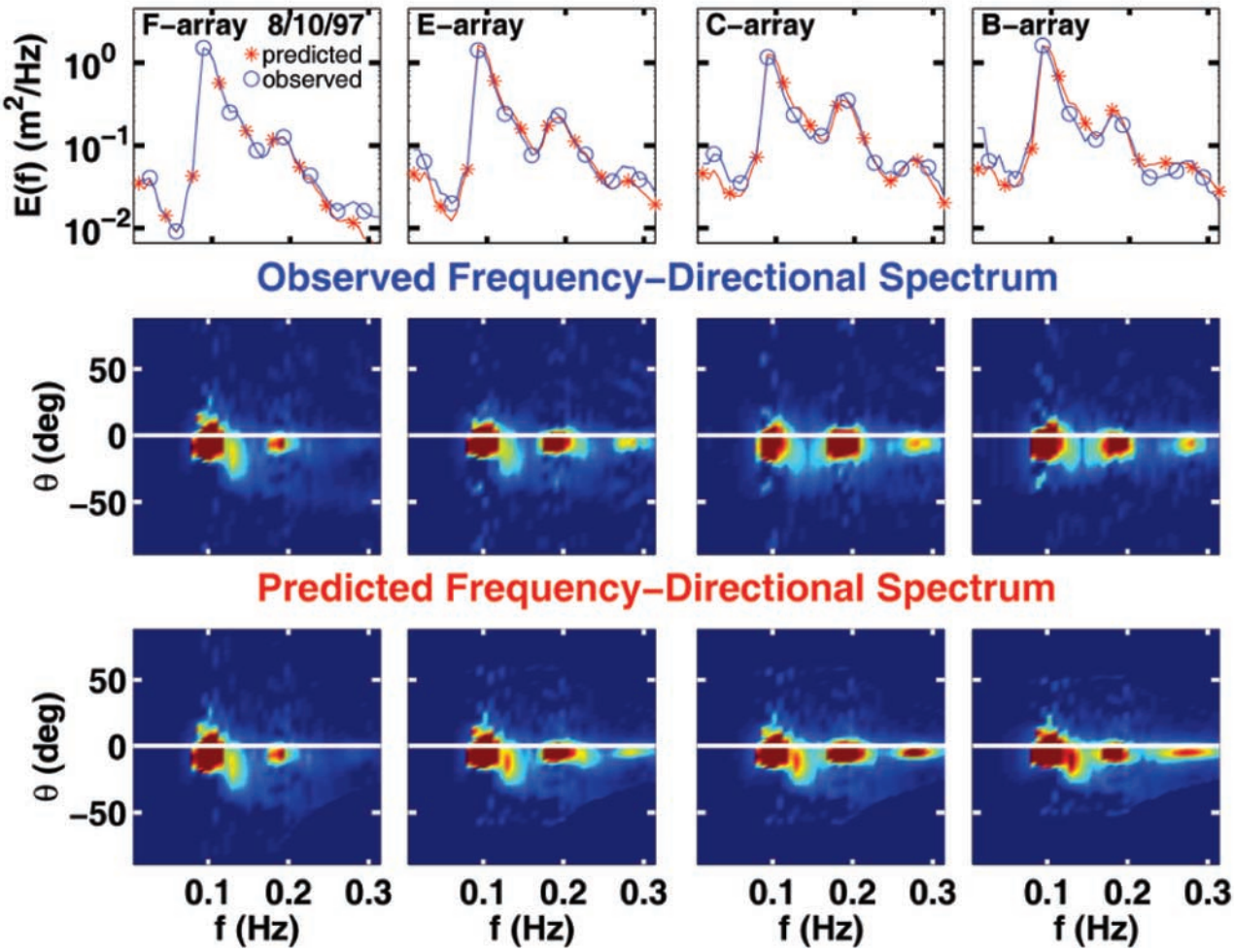

Figure 2. Comparison of observed with predicted wave spectra evolution on 10 August 1997. From left to right, results are shown for the F, E, C, and B arrays (locations are indicated in Figure 1a). Upper panels: observed (blue) and predicted (red) frequency spectra. Middle and lower panels: observed and predicted frequency-directional spectra, respectively. The color scale is linear from low (blue) to high (red) spectral levels. To enhance the harmonic structure in the two-dimensional color images the spectral levels were weighted by the frequency f. Slight differences at high frequencies between the observed spectrum and the initial model spectrum at the F-array (upper left panel) result from the truncation of the model domain for large alongshore wavenumbers.

incidence angles are reduced by refraction, the propagation direction θ of a component with frequency f and alongshore wavenumber l can be approximated by

$$\theta = \frac{l\sqrt{gh}}{2\pi f} + O\left((\kappa h)^2\right). \tag{15}$$

It follows from equation (15) and the interaction rules in equation (1) that the sum interaction of a pair of components with frequencies and directions (f_1, θ_1) and (f_2, θ_2) forces a wave component with the sum frequency and a direction that is given approximately by the weighted average of the angles θ_1 and θ_2:

$$f_3 = f_1 + f_2 \tag{16a}$$

$$\theta_3 \approx \frac{f_1\theta_1 + f_2\theta_2}{f_1 + f_2}. \tag{16b}$$

The strongest interactions involve two components within the spectral peak, and thus in agreement with the observations, the most energetic excited waves are predicted to have a frequency of about $2f_p$ and to be aligned directionally with the dominant f_p waves (Figure 2).

[27] Predictions of sea surface skewness and asymmetry, obtained by integrating the real and imaginary parts of the bispectrum [see *Elgar and Guza*, 1985], agree well with observations (Figure 3). Predicted skewness values are $\sim$10–20% higher than the observed values but reproduce the observed cross-shore evolution, including the maximum near the crest of the sand bar (Figure 3a, cross-shore distance 320 m). The predicted asymmetry is in excellent agreement with the observations (Figure 3b). Seaward of the bar crest the asymmetry is positive, characteristic of pitched-forward waves [*Elgar and Guza*, 1985] and harmonic growth (i.e., the last term on the right-hand side of equation (5a) is positive). The asymmetry is negative (and

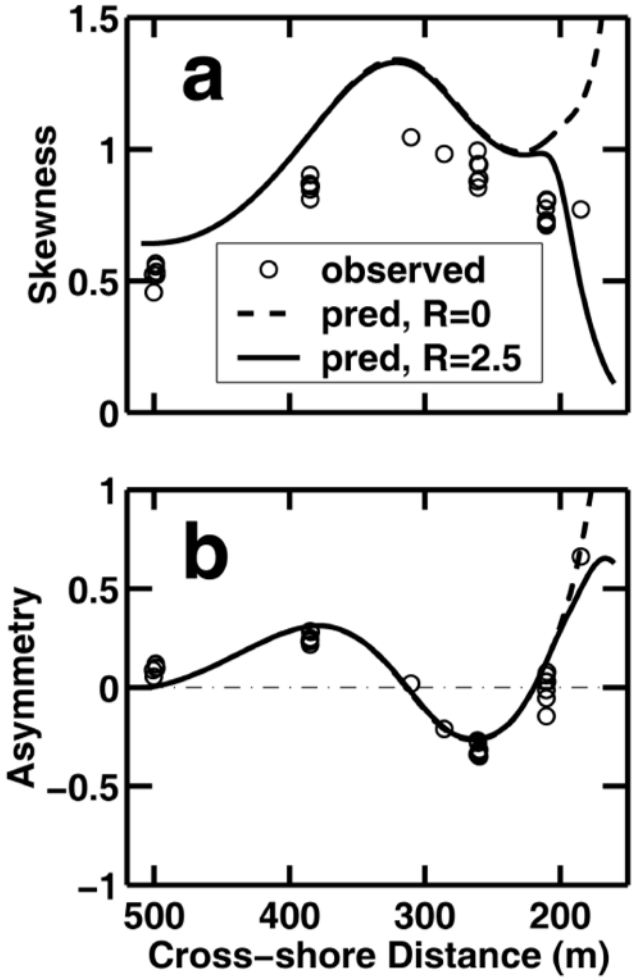

Figure 3. Observed (circles) and predicted (solid curves) sea surface elevation (a) skewness and (b) asymmetry versus cross-shore distance on 10 August 1997. Multiple estimates at the cross-shore locations of the alongshore arrays give an indication of the statistical uncertainty in these estimates. Model predictions obtained with the alternative quasi-normal closure approximation ($R = 0$) are indicated with dashed curves.

energy transfers reverse, equation (5a)) over the down slope region of the beach profile inshore of the bar crest (220–310 m), and increases sharply to positive values farther inshore on the steep beach face.

[28] Seaward of the shallowest instrument, predictions obtained with the quasi-normal closure approximation $C^4 = 0$ (dashed curves in Figure 3) are nearly identical to those obtained with the relaxation closure model because the relaxation term in equation (7) tends to zero outside the surf zone where the damping term D_2 is small. Similarly, differences between the spectra $E(f, \theta)$ predicted by the two closure models (not shown) are negligible at all four arrays. The excellent agreement with the observations confirms that the quasi-normal approximation describes accurately the wave shoaling evolution in regions of weak nonlinearity, consistent with earlier model-data comparisons by *Norheim et al.* [1998]. However, inshore of the instrumented transect ($x < 200$ m in Figure 3) where breaking of larger waves occurs, the two closure models diverge sharply. The quasi-normal closure model predicts a strong amplification of the skewness and asymmetry towards the shore that is not observed (Figure 3 and Appendix A), indicating that the fourth-order cumulant plays an important role in maintaining near-Gaussian statistics in regions of strong nonlinearity.

[29] On 9 September the wave field at the F-array was bimodal with a dominant swell (H_s = 1.0 m) with peak frequency f_p = 0.08 Hz arriving from a southerly (−20°) direction, and a much less energetic (about a factor of 10) secondary wave system with a 0.18 Hz peak frequency arriving from a northerly (+30°) direction (Figure 4). Similar to the 10 August case, the model predicts the observed development of harmonic peaks at $2f_p$ and $3f_p$ that are aligned directionally with the dominant southerly swell. The direction of the northerly component shifts owing to refraction, but the energy is unchanged during shoaling. At the shallowest B-array the predicted energy of the northerly waves is ∼40 % larger than observed, possibly owing to the tendency of the weakly dispersive model to overshoal short wavelength components of the spectrum. Predicted sum interactions result in directional distributions $S(\theta)$ at harmonic frequencies (Figures 5b and 5c) that are narrower than the distribution at the dominant swell frequency (Figure 5a). At frequency $3f_p$ the initial broad bimodal $S(\theta)$ with equal contributions of northerly (free, $\theta \approx +30°$) and southerly (harmonic, $\theta \approx -20°$) components observed at the F-array (dotted curve in Figure 5c) is transformed in the model prediction to a narrow distribution dominated by southerly harmonic components at the C-array (asterisks on dark curve), as is observed (circles on light curves). Although the predicted and observed $S(\theta)$ are generally in good agreement, the predicted slight refraction of the mean direction toward normal incidence (about 3° at f_p, Figure 5a) is not observed, suggesting that neglected alongshore variations in depth or incident wave conditions may contribute errors to the model predictions. The spatial patterns and agreement between observed and predicted third moments (not shown) are similar to the 10 August results (Figure 3).

[30] The cross-interaction between the southerly swell (0.08 Hz) and northerly seas (0.18 Hz), transferring energy to a component with frequency 0.26 Hz and direction between the swell and sea (equation (16)) is theoretically weak (and is not observed, Figure 4) because the northerly wave energy is low. The cross-interaction between two wave systems with approximately equal energy and traveling in different directions was examined with data from a large directional basin [*Elgar et al.*, 1993]. The test section of the basin consisted of a plane beach sloping from 0.40 to 0.16 m depth over a distance of 7.2 m. Frequency-directional spectra were estimated from two alongshore arrays of wave height gauges located in 0.40 and 0.16 m depth (Figures 6b and 6c) (see *Elgar et al.*, 1993 for details of the experiment and analysis). The model was initialized with the measured $E(f, \theta)$ at the offshore array.

[31] The wave spectrum measured offshore in 0.40 m depth (H_s = 0.09 m) was bimodal with approximately equal energy in two peaks with frequencies f_1 = 0.42 Hz and f_2 = 0.57 Hz (Figure 6a), and mean propagation directions of 0° and +20°, respectively (Figure 6b). In 0.16 m depth, at about the outer edge of the surf zone, the predicted spectral

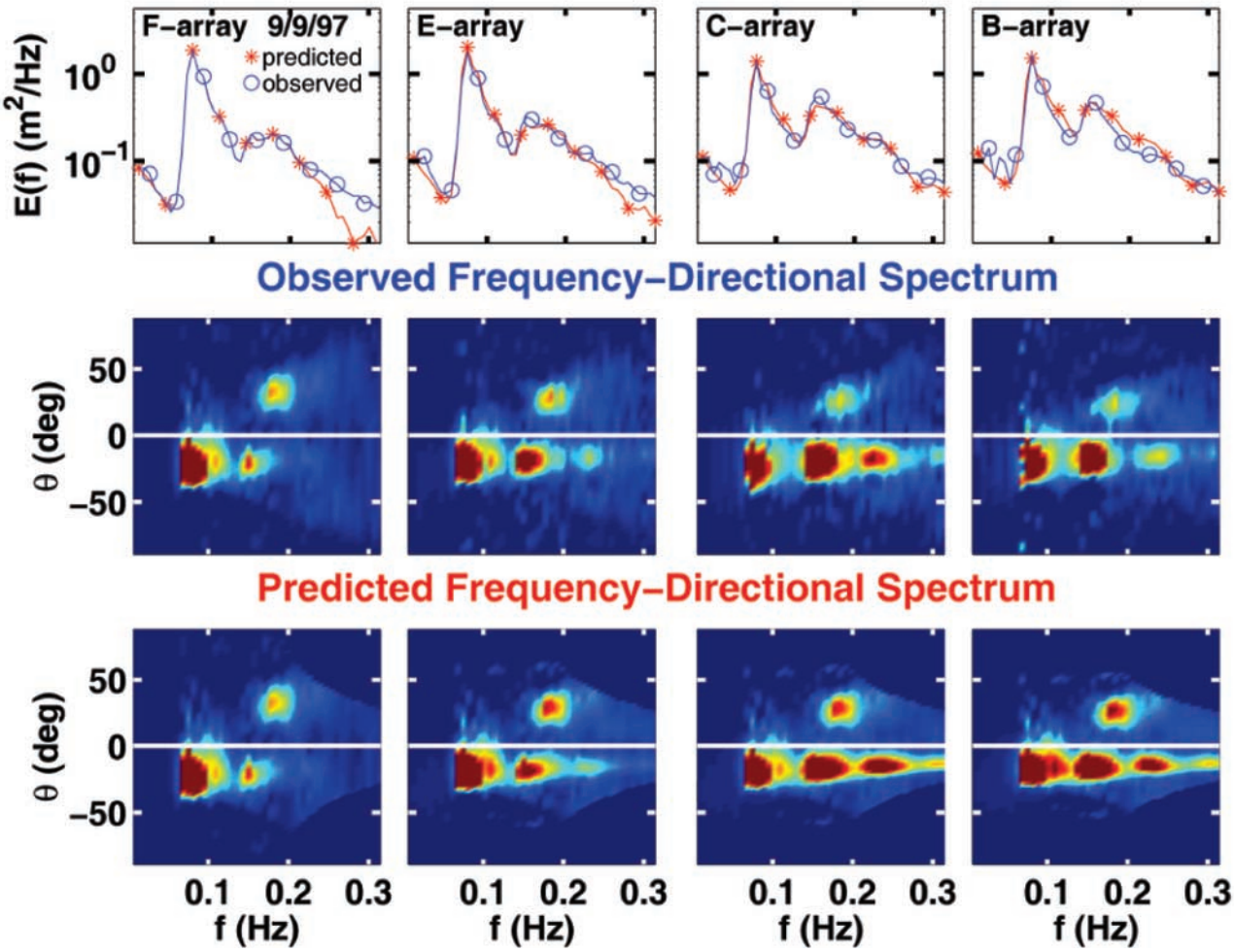

Figure 4. Comparison of observed with predicted wave spectra evolution on 9 September 1997 (same format as Figure 2.).

level (Figure 6a) and direction (Figure 6e) of the lower-frequency peak are unchanged, whereas the higher-frequency peak energy is reduced by ~25% (Figure 6a) and the direction is refracted toward normal incidence (+12°, Figure 6f), in good agreement with the measurements.

[32] Predicted energy levels, frequencies, and directions of the nonlinearly forced high-frequency ($2f_1$, $f_1 + f_2$, and $2f_2$) peaks also agree well with the measurements (see the solid red and blue curves in Figures 6a and 6g–6i). The largest nonlinearly forced peak, at frequency $f_1 + f_2$, with a direction approximately midway between the directions of the f_1 and f_2 peaks (Figure 6d), results from the cross-interaction of the two wave systems. The high spectral level of the $f_1 + f_2$ waves, relative to the $2f_1$ and $2f_2$ waves, can be explained with equation (3). For simplicity, consider the sum interactions of a bimodal spectrum with two well-separated peaks f_1 and f_2 with equal energy and equal spectral width. From symmetry considerations it follows that the number of cross-interaction terms (involving one component from each wave system) is twice the number of self-interaction terms for each wave system. Thus if the frequency and alongshore wavenumber separation of the two peaks is sufficiently small that differences in resonance mismatch and coupling coefficient can be neglected, then the approximate distribution of nonlinear energy transfers to the $2f_1$, $f_1 + f_2$, and $2f_2$ peaks is 25%, 50%, and 25%.

5. Spectral Evolution Inside the Surf Zone

[33] Outside the surf zone the Boussinesq model is based on a rigorous description of the energy-conserving physics without any empirical coefficients and reproduces accurately the observed evolution of $E(f, \theta)$ and of wave skewness and asymmetry. However, inside the surf zone dissipation is important, and the assumption of weak nonlinearity may be violated. The crude model parameterizations of the effects of dissipation and strong nonlinearity were tuned empirically by determining an optimal combination of values of the free parameters γ, b, and R that minimizes prediction errors for the DUCK94 data set (Appendix A). Here, the robustness of these approximations is illustrated by comparing model predictions with observations during the peak of a severe nor'easter storm on 15 October 1994, when the majority of the instruments were within the surf zone (Figure 7). The model was initialized with the observed $E(f, \theta)$ at the 8 m depth array. The observed decay of H_s from 3.4 m in 8 m depth to 0.8 m in 1 m depth is reproduced well by the model (Figure 7b). However, the predicted gradual decay does not

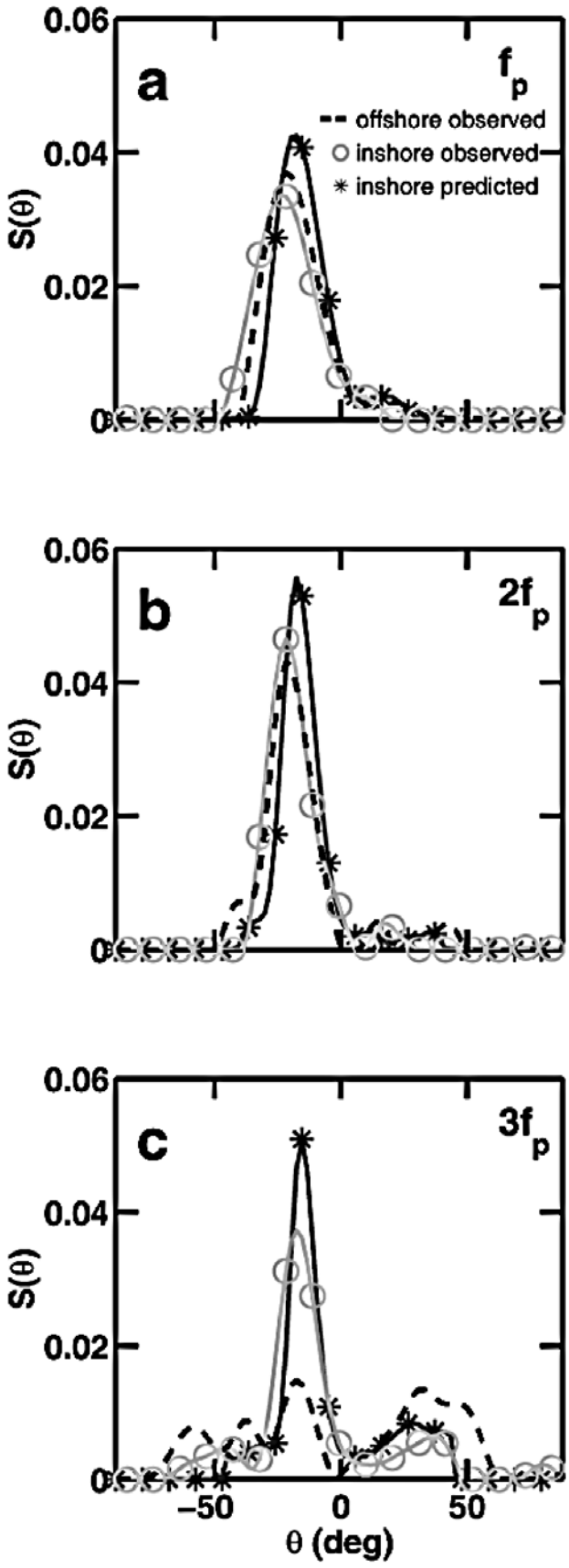

capture the observed strong localized dissipation over the crest of the sand bar (cross-shore distance ≈300 m), where H_s decreased from 1.9 to 1.2 m over a distance of only 20 m. The model predicts accurately the observed evolution of the frequency spectrum $E(f)$, in particular the dramatic broadening of the initially narrow spectrum (f_p = 0.09 Hz) with a pronounced harmonic peak ($2f_p$ = 0.18 Hz) to an almost uniform spectrum in the inner surf zone (Figures 7f–7i). Near the shore (Figure 7i) the model predicts a dip in $E(f)$ at the peak frequency that is not observed. This discrepancy results from the crude parameterization of the fourth cumulant term in the third-order closure scheme (equation (7)), causing an overshoot in the nonlinear energy transfers from the spectral peak to other parts of the spectrum [e.g., *Orszag*, 1970]. This instability can be suppressed by increasing the bispectrum relaxation coefficient R, but at the expense of degraded predictions of third-order statistics (see Appendix A, Figure A1b).

[34] Skewness predictions (Figure 7c) are within 10–30% of the observed values, except for the bar crest region where the predictions are ~60% lower than the observations. The model reproduces qualitatively the observed evolution of asymmetry (Figure 7d), increasing from small values offshore to a maximum over the sand bar, decreasing to small values in the downslope region inshore of the bar crest, and increasing again on the beach face. Errors in the asymmetry predictions range from less than 15% at offshore locations to as much as 60% near the shoreline.

[35] The predicted mean wave directions (within 4° of normal incidence across the entire transect) are consistent with the observations (not shown), but the model underpredicts the directional spread, in particular on the sand bar where the predicted spread is ~40% smaller than the observed spread (Figure 7e). Similar discrepancies were found in most other surf zone observations. For example, the largest waves of the SandyDuck experiment were observed on 19 October 1997 (Figure 8, H_s = 3.0 m at the F-array). In this case the model initial conditions ($E(f, \theta)$ at the F-array) consisted of a steep wind sea (f_p = 0.10 Hz) with a broad unimodal directional distribution centered at a small northerly (≈ +5°) angle (dashed curves in Figure 8). Observed and predicted frequency spectra and directional distributions (at frequencies f_p and $2f_p$) are compared at the inshore C-array where most of the incident wave energy is dissipated (H_s = 1.6 m). The predicted $E(f)$ (Figure 8a) and $S(\theta)$ at the dominant sea frequencies (e.g., Figure 8b) agree well with the observations, but the predicted $S(\theta)$ at higher frequencies are about a factor of 2 narrower than the observed distributions (e.g., Figure 8c). Both the observed and predicted $S(\theta)$ at high frequencies have maxima near the dominant sea direction, but the observed energy at large oblique (up to 60°) northerly and southerly angles is not

Figure 5. (opposite) Directional distributions of wave energy observed (circles on light curves) and predicted (asterisks on dark curves) at the C-array on 9 September 1997. Distributions are shown at frequencies: (a) f_p, (b) $2f_p$, and (c) $3f_p$ where f_p = 0.08 Hz (Figure 4). Dashed curves indicate the initial distributions observed at the F-array. Predicted distributions exclude high frequency components at large angles, whereas the observed distributions include all incidence angles between −90° and +90°.

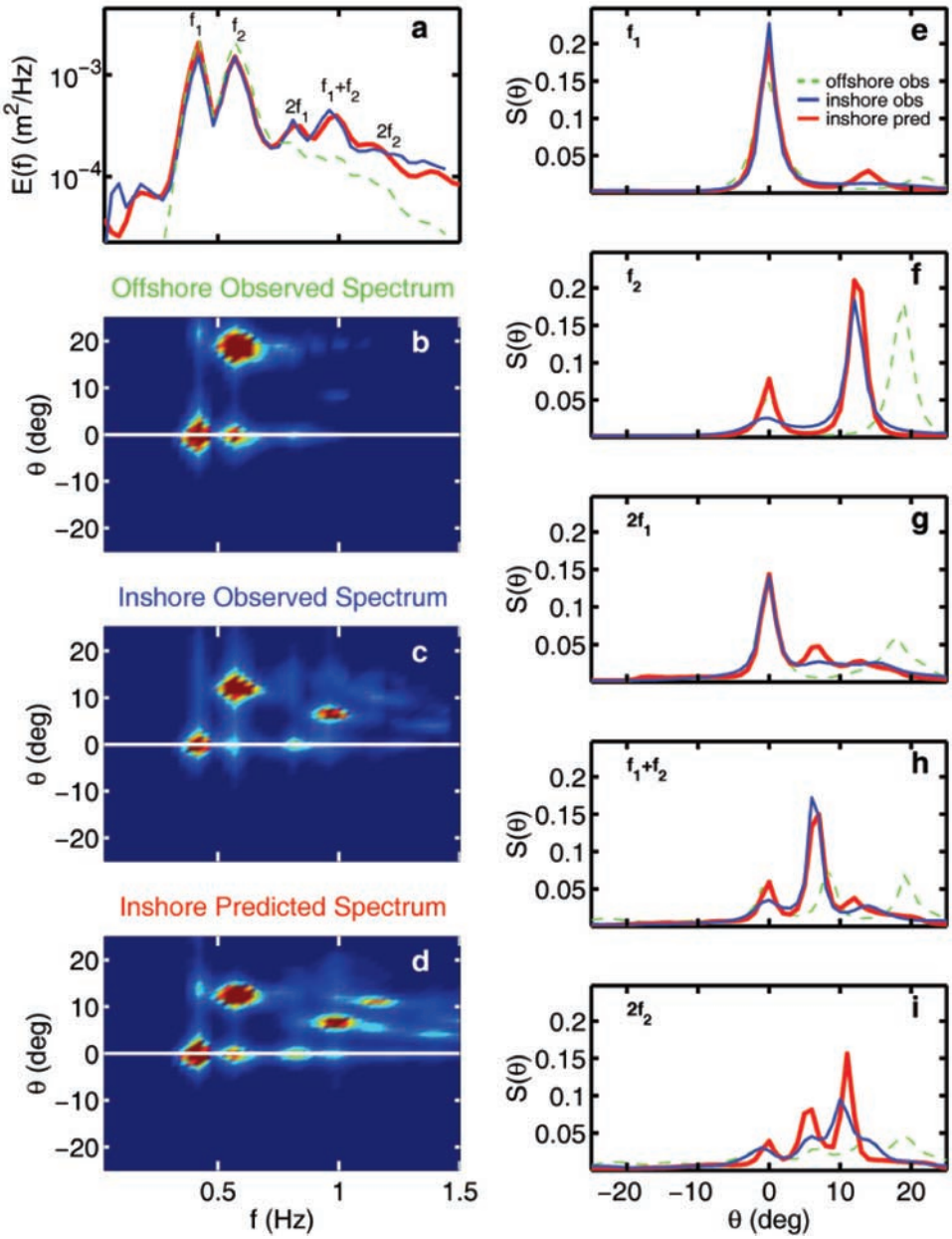

Figure 6. Laboratory measurements [*Elgar et al.*, 1993] and model predictions of the self- and cross-interactions of two wave systems traveling in different directions. (a) Measured (blue) and predicted (red) frequency spectrum in 0.16 m depth. The dashed green curve is the initial measured spectrum (0.40 m depth). The color panels show (b) the initial bimodal frequency-directional spectrum in 0.40 m depth, and the (c) measured and (d) predicted shoaled spectrum in 0.16 m depth (same format as Figure 2). Figures 6e–6i show the initial measured (dashed green curves), inshore measured (solid blue), and inshore predicted (solid red) directional distributions at the incident wave peak frequencies f_1 = 0.42 Hz and f_2 = 0.57 Hz and the associated sum frequencies.

predicted by the model. The cause of this directional broadening is unknown. Neglected higher-order quartet wave-wave interactions, a well-known mechanism for scattering wave energy at large oblique angles in deep water [e.g., *Hasselmann*, 1962], may be important to the evolution of steep high-frequency components. Wave diffraction associated with spatial fluctuations in the random onset of wave breaking also may cause a directional broadening of waves in the surf zone, as may edge waves trapped on the sand bar [*Bryan and Bowen*, 1996] or along the shoreline [*Eckart*, 1951; *Ursell*, 1952]. Further studies are needed to understand and improve the parameterization of directional spreading in the surf zone.

6. Summary

[36] The shoaling evolution of the wave frequency-directional spectrum was investigated with field and laboratory

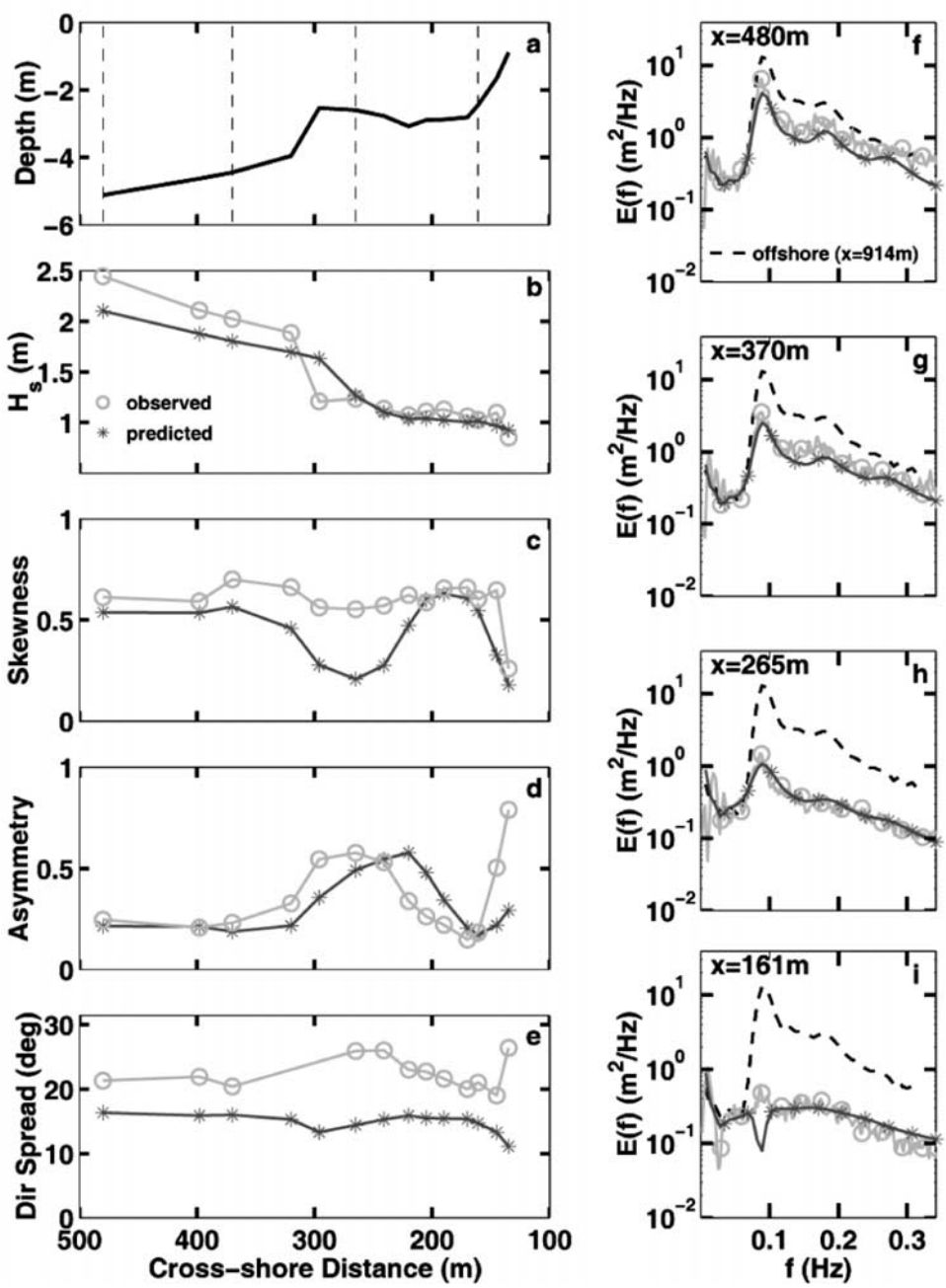

Figure 7. Comparison of observed (circles on light curves) with predicted (asterisks on dark curves) wave transformation across the surf zone on 15 October 1994. Left panels: (a) water depth, (b) significant wave height, (c) skewness, (d) asymmetry, and (e) directional spread versus cross-shore distance. The model was initialized in 8 m depth (cross-shore location 914 m) where the significant wave height was 3.4 m. Right panels show frequency spectra at four locations (indicated with dashed lines in Figure 7a): (f) outer surf zone, (g) seaward of the sand bar, (h) on the bar crest, and (i) inshore of the bar crest. For reference the initial spectrum observed in 8 m depth is indicated in each panel with a dashed curve.

observations and a numerical model based on a stochastic formulation of the Boussinesq equations. Detailed measurements of wave shoaling evolution across a natural beach were acquired in two field experiments using a cross-shore transect and multiple coherent alongshore arrays of pressure gauges and current meters. A coupled set of evolution equations for the wave spectrum and bispectrum were integrated numerically, accounting for linear shoaling and refraction and nonlinear energy exchanges in triad interactions. A simple parameterization of surf zone damping with a frequency-dependent dissipation rate was adopted from earlier studies, and strong nonlinearity was parameterized using a relaxation to Gaussian statistics. Adjustable coefficients in this parameterization were calibrated with the observed evolution of waves across the surf zone.

[37] Model predictions of the frequency-directional spectrum in low to moderate conditions with nonbreaking

waves reproduce the observed development of harmonic components traveling in directions that are aligned with the dominant swell direction. Predicted spectral levels, frequencies, and directions of the harmonic peaks are in good agreement with the field observations. The model also reproduces accurately the cross-interaction of a bimodal (in frequency and direction) incident wave field reported in an earlier laboratory study. Predictions of sea surface elevation skewness and asymmetry, third-order moments that are believed to be important to sediment transport, also agree well with observations outside the surf zone.

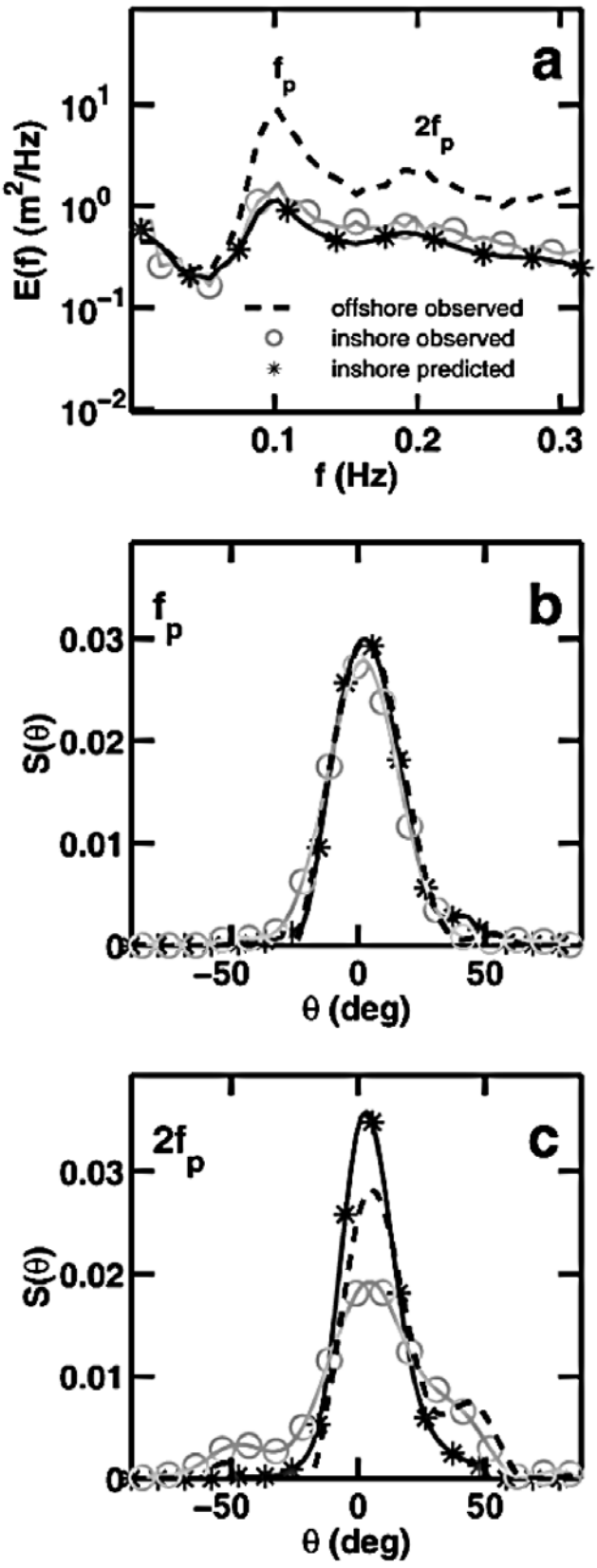

Figure 8. (opposite) Observed (circles on light curves) and predicted (asterisks on dark curves) spectra at the C-array, situated well inside the surf zone on 19 October 1997. (a) $E(f)$, (b) $S(\theta)$ at $f_p = 0.10$ Hz, and (c) $S(\theta)$ at $2f_p$. Dashed curves indicate the initial spectrum and directional distributions observed at the F-array. Predicted distributions exclude high frequency components at large angles, whereas the observed distributions include all incidence angles between −90°and +90°.

[38] Comparisons of model predictions with observations in high-energy surf zone conditions demonstrate the robustness of the parameterization of wave breaking effects, but also indicate some shortcomings. The observed evolution across the surf zone of initially narrow frequency spectra with distinct harmonic peaks to broad, featureless spectra, is reproduced well by the model. Although wave breaking does not appear to affect the mean propagation directions of incident waves and harmonic components significantly, the observed increase in directional spreading (as much as a factor of 2 at high frequencies) across the surf zone is not predicted. Predictions of wave skewness and asymmetry in the surf zone are in fair agreement with the observations.

Appendix A: Calibration of Surf Zone Coefficients

[39] The parameterization of surf zone wave breaking in the present model contains two adjustable coefficients γ and b (equation (12)) that determine the bulk dissipation rate and one coefficient R (equation (7)) that controls the rate at which nonlinear phase coupling between triads of wave components is lost in the breaking process. Optimal values for these coefficients were determined empirically using field measurements of wave evolution across the surf zone collected in the DUCK94 experiment (Figure 1b). Model predictions were compared with observations from 125 1-hour-long data records collected at low tide in moderate to energetic conditions (incident $H_s > 1.25$ m) when significant wave energy losses were observed across the shallow sand bar. To reduce the significant computational effort required to model this large data set for a wide range of coefficient values, the computations were performed for unidirectional incident waves ($l = 0$). Limited model tests with full frequency-directional spectra indicate that the predicted evolution of bulk wave statistics across the surf zone is insensitive to the directional properties of incident waves. For each case the initial frequency spectrum $E(f)$ was estimated based on measurements at the farthest offshore instrument (Figure 1b).

[40] The accuracy of the model predictions is quantified here with root-mean-square averages of errors in predicted

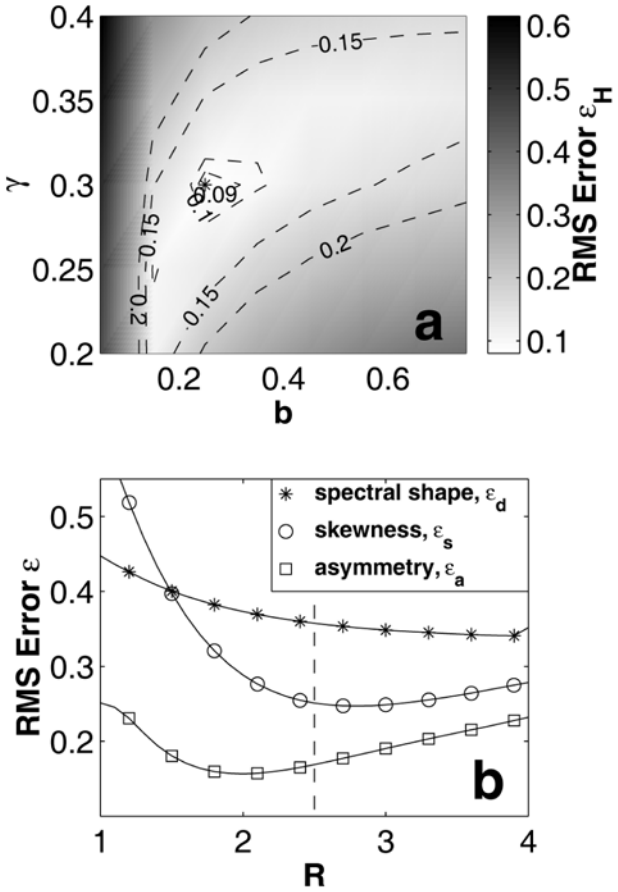

Figure A1. Calibration of empirical coefficients in the surf zone parameterization with data from the DUCK94 experiment. (a) Root-mean-square average ε_H of the normalized wave height model error (equation (A1a)) as a function of the values of the coefficients γ and b. The optimal combination of γ and b (i.e. minimum ε_H) is indicated with an asterisk. (b) Root-mean-square model errors of wave skewness, asymmetry, and normalized spectral shape (equations (A1b), (A1c), and (A1d), respectively) versus the value of coefficient R. The subjective choice of an optimal R for which all three error measures are small is indicated with a dashed line.

wave heights (ε_H), skewness (ε_s), asymmetry (ε_a), and the shape of the frequency spectrum (ε_d), defined as:

$$\varepsilon_H \equiv \sqrt{\frac{1}{N}\sum\left(\frac{H_{s,pred}-H_{s,obs}}{H_{s,obs}}\right)^2} \tag{A1a}$$

$$\varepsilon_s \equiv \sqrt{\frac{1}{N}\sum\left(s_{pred}-s_{obs}\right)^2} \tag{A1b}$$

$$\varepsilon_a \equiv \sqrt{\frac{1}{N}\sum\left(a_{pred}-a_{obs}\right)^2} \tag{A1c}$$

$$\varepsilon_d \equiv \sqrt{\frac{1}{N}\sum\frac{\int df\left(\tilde{E}_{pred}(f)-\tilde{E}_{obs}(f)\right)^2}{\int df\tilde{E}_{obs}(f)^2}}, \tag{A1d}$$

where the summation is over all 125 cases and all (up to 13) operating instruments (excluding the farthest offshore sensor where the model was initialized), yielding a total of N = 1415 error estimates. Wave height errors ($H_{s,\mathrm{pred}} - H_{s,\mathrm{obs}}$) were normalized by the observed wave height ($H_{s,\mathrm{obs}}$) to weight equally the relative error in each observation. The integral in equation (A1d) is over the swell-sea frequency range, and the spectrum $\tilde{E}(f)$ is normalized by the variance.

[41] The coefficient R in the bispectrum evolution equation does not affect the evolution of total wave energy. Therefore the wave height error ε_H was minimized for all possible combinations of the remaining coefficients γ and b (at intervals of 0.05 and 0.1, respectively) within their probable range $0.2 < \gamma < 0.4$ and $0.05 < b < 0.75$, yielding a minimum error $\varepsilon_H = 0.08$ for $\gamma = 0.30$ and $b = 0.25$ (Figure A1a). Having determined optimal γ and b values, the model was run again through the entire data set for $1 < R < 4$. The skewness and asymmetry errors (Figure A1b) are sensitive to the coefficient R that controls the rate at which the wave field relaxes to a Gaussian state with zero skewness and asymmetry. Minimum ε_s and ε_a were found for R values of 2.8 and 2.0, respectively. The spectral shape error ε_d appears to be less sensitive to the value of R (Figure A1b). On the basis of these results a value of $R = 2.5$ was chosen with errors $\varepsilon_s = 0.25$, $\varepsilon_a = 0.17$, and $\varepsilon_d = 0.36$.

[42] Using optimal coefficient values $\gamma = 0.30$, $b = 0.25$, and $R = 2.5$, the observed significant wave heights, skewness, and asymmetry are predicted reasonably well over a wide range of conditions (Figure A2). Observed and predicted wave heights and asymmetry are approximately randomly scattered about lines of one-to-one correspondence (Figures A2a and A2c), although large values of skewness are systematically overpredicted by $\sim$10–20% (Figure A2b).

[43] The relaxation closure affects the predicted evolution across the surf zone. For the 15 October 1994 storm (section 5) predictions of frequency spectra well inside the surf zone for $R = 2.5$ (the optimized closure) and $R = 5$ (a faster relaxation rate) are similar and in good agreement with the observations (Figure A3). In contrast, for $R = 0$ (quasi-normal closure) the predicted spectrum has a pronounced harmonic structure that is not observed (Figure A3). The serious deficiency of the quasi- normal closure in the surf zone also is evident from large errors in the predicted skewness and asymmetry moments (not shown; the predicted values are as large as 5, whereas the observed values are usually less than 1).

Appendix B: Discretization of the Spectrum and Bispectrum

[44] For efficient numerical evaluation of the evolution equations (5a, 5b) it is advantageous to account for symmetries in the spectrum and bispectrum. From the symmetry relations

$$E(-\omega,-l) = E(\omega,l) \tag{B1a}$$

$$\begin{aligned} B(\omega_1,l_1,\omega_2,l_2) &= B(\omega_1,l_1,-\omega_1-\omega_2,-l_1-l_2) \\ &= B(\omega_2,l_2,-\omega_1-\omega_2,-l_1-l_2) \\ &= B(\omega_2,l_2,\omega_1,l_1) \\ &= B^*(-\omega_1,-l_1,-\omega_2,-l_2), \end{aligned} \tag{B1b}$$

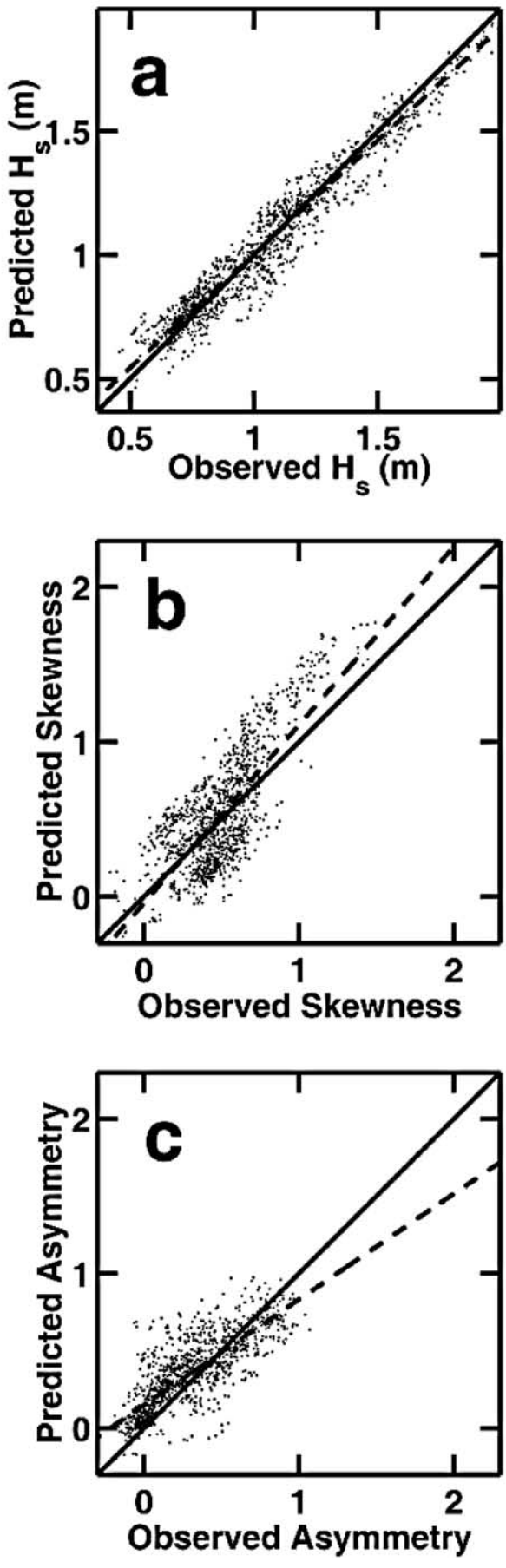

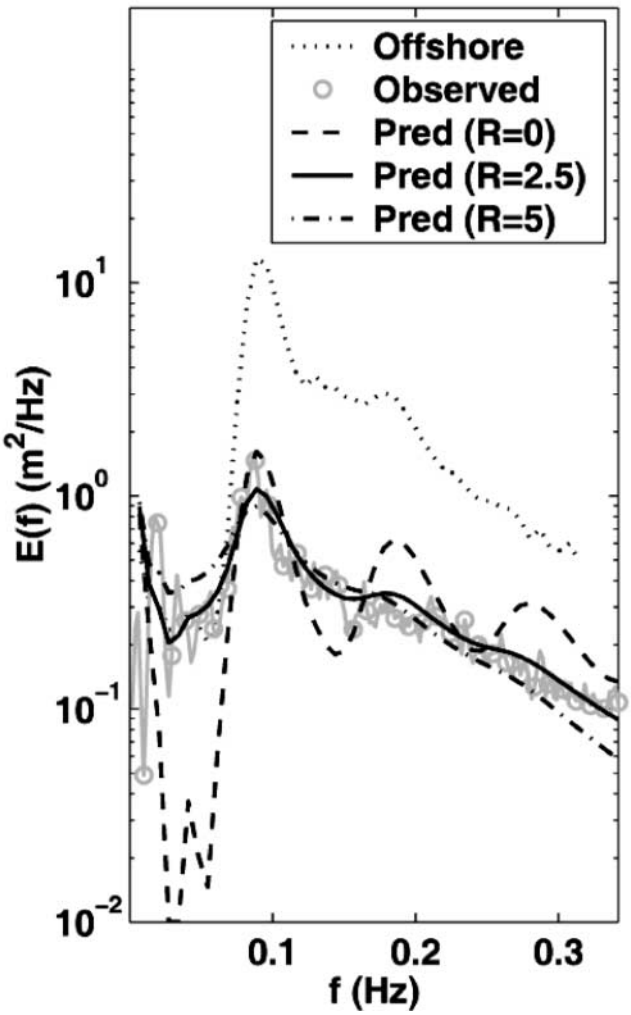

Figure A3. Comparison of observed (circles on light curve) with predicted (dark curves) frequency spectra well inside the surf zone for three values of the closure parameter R. The data were collected on 15 October 1994 in 2.5 m depth with an offshore significant wave height of 3.4 m (same case and cross-shore location as Figure 7h). For reference the initial model spectrum observed at the outer edge of the surf zone is indicated with a dotted curve.

where the asterisk denotes the complex conjugate, it follows that nonredundant regions of the spectrum and bispectrum can be defined as [e.g., *Chandran and Elgar*, 1990]

$$0 < \omega < \infty, -\infty < l < \infty \qquad \text{(B2a)}$$

Figure A2. (opposite) Predicted versus observed (a) significant wave height, (b) skewness, and (c) asymmetry, for model computations using the calibrated set of coefficient values $\gamma = 0.3$, $b = 0.25$, and $R = 2.5$. The model, neglecting directionality, was initialized with measurements at the farthest offshore sensor in the DUCK94 transect (Figure 1b). Each dot represents a comparison for a 1-hour-long data record at one of the inshore instruments. Dashed and solid lines indicate a best fit line to the scatter diagram based on linear regression analysis and a one-to-one correspondence line, respectively.

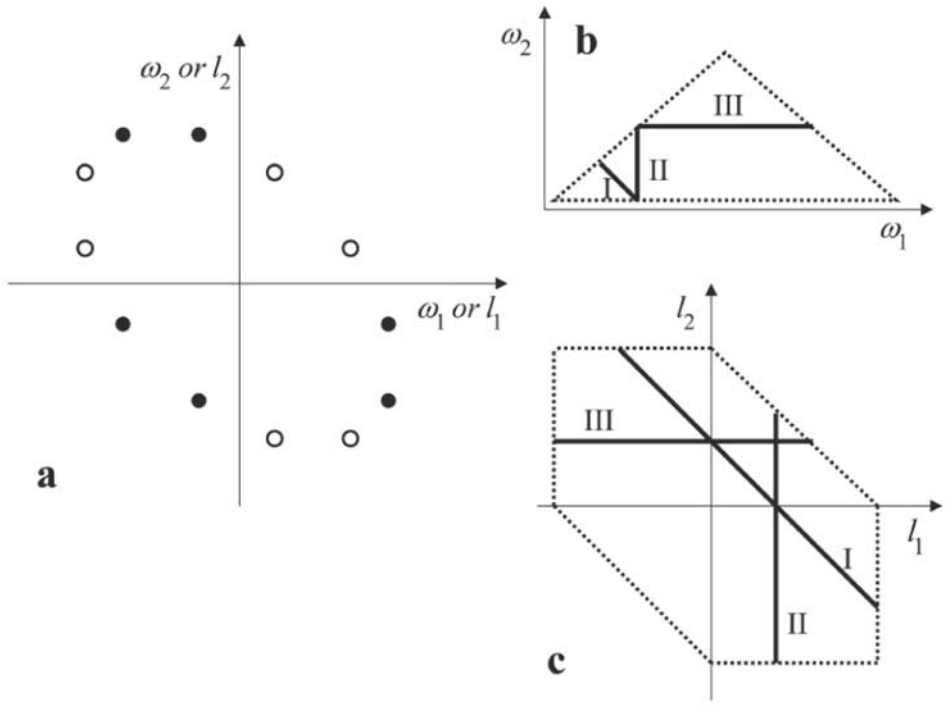

Figure B1. (a) Schematic of symmetries in the bispectrum. Open and filled circles indicate six equal and six complex conjugate bispectrum values. (b, c) Integration paths (equation (B3)) through the nonredundant region of the bispectrum domain. Dotted lines indicate the minimum and maximum frequencies and alongshore wavenumbers in the model domain.

$$0 < \omega_2 < \omega_1 < \infty, -\infty < l_1, l_2 < \infty \tag{B2b}$$

(Figure B1a). Using the relations in equation (B1b), the integral in equation (5a) can be mapped into the nonredundant region (equation (B2b))

$$\begin{aligned}
&\int_{-\infty}^{\infty} dl' \int_{-\infty}^{\infty} d\omega' IM\{B(\omega', l', \omega - \omega', l - l')\} \\
&= 2 \int_{-\infty}^{\infty} dl' \Bigg\{ \underbrace{\int_{\omega/2}^{\omega} d\omega' IM\{B(\omega', l', \omega - \omega', l - l')\}}_{\text{I}} \\
&\quad - \underbrace{\int_{0}^{\omega} d\omega' IM\{B(\omega, l, \omega', l')\}}_{\text{II}} - \underbrace{\int_{\omega}^{\infty} d\omega' IM\{B(\omega', l', \omega, l)\}}_{\text{III}} \Bigg\},
\end{aligned} \tag{B3}$$

so that the evolution equations (5a, 5b) depend only on the spectrum and bispectrum in the nonredundant regions defined in equations (B2a) and (B2b).

[45] The spectrum $E(\omega, l)$ is discretized with N_ω (positive) frequencies ($\delta\omega, 2\delta\omega, \ldots, N_\omega\delta\omega$), and $2N_l + 1$ alongshore wavenumbers ($-N_l\delta l, \ldots, -\delta l, 0, \delta l, \ldots, N_l\delta l$). The corresponding discretized bispectrum $B(\omega_1, l_1, \omega_2, l_2)$ contains $N_\omega^2/4$ frequency pairs within a triangle $\delta\omega \le \omega_2 \le \omega_1 < \omega_1 + \omega_2 \le N_\omega\delta\omega$ (Figure B1b) and $3N_l^2 + 3N_l + 1$ alongshore wavenumber pairs within a hexagon $-N_l\delta l \le l_1, l_2, l_1 + l_2 \le N_l\delta l$ (Figure B1c). Thus, the total number of triads in the model equals $(N_\omega^2/4)[3N_l^2 + 3N_l + 1]$.

[46] The integrals on the right-hand side of equation (B3) are evaluated by summing $IM\{B(\omega_1, l_1, \omega_2, l_2)\}$, multiplied by the corresponding bandwidth ($\delta\omega\delta l$ for $\omega_1 \neq \omega_2$ and $\delta\omega\delta l/2$ for $\omega_1 = \omega_2$), along the integration planes $\omega_1 + \omega_2 = \omega$, $l_1 + l_2 = l$ (I), $\omega_1 = \omega$, $l_1 = l$ (II), and $\omega_2 = \omega$, $l_2 = l$ (III) (Figures B1b and B1c). Nonlinear energy transfers balance exactly within each triad, and only those triads for which all frequencies and alongshore wavenumbers fall within the model domain are included. Consequently, the model (in the absence of dissipation) conserves energy.

[47] **Acknowledgments.** This research was supported by the Coastal Dynamics Program of the Office of Naval Research, the National Oceanographic Partnership Program (NOPP), and the National Science Foundation (Physical Oceanography). The nearshore arrays in the DUCK94 and Sandy-Duck field experiments were deployed and maintained by the staff of the Scripps Institution of Oceanography Center for Coastal Studies. We thank Britt Raubenheimer, Edie Gallagher, and Falk Feddersen for their contributions to the field experiments. Excellent logistical support, bathymetry and instrument location surveys, and array data in 8 m depth were provided generously by the Field Research Facility of the U.S. Army Engineer Waterways Experiment Station's Coastal Engineering Research Center. Permission to use these data is appreciated. We thank Michael Briggs for his contributions to the laboratory experiments and the anonymous reviewers and John Trowbridge for helpful comments. WHOI Contribution 10620.

References

Agnon, Y., and A. Sheremet, Stochastic nonlinear shoaling of directional spectra, *J. Fluid Mech.*, *345*, 79–99, 1997.

Battjes, J. A., and J. P. F. M. Janssen, Energy loss and set-up due to breaking of random waves, in *Proceedings of the 16th International Conference on Coastal Engineering*, pp. 569–587, Am. Soc. of Civ. Eng., New York, 1978.

Bryan, K. R., and A. J. Bowen, Edge wave trapping and amplification on barred beaches, *J. Geophys. Res.*, *101*, 6543–6552, 1996.

Chandran, V., and S. Elgar, Bispectral analysis of 2-D random processes, *IEEE Trans. Acoust. Speech Signal Process.*, *38*, 2181–2186, 1990.

Chen, Q., J. T. Kirby, R. A. Dalrymple, A. B. Kennedy, and A. Chawla, Boussinesq modeling of wave transformation, breaking, and runup., II, 2D, *J. Waterw. Port Coastal Ocean Eng.*, *126*, 48–56, 2000.

Chen, Y., R. T. Guza, and S. Elgar, Modeling spectra of breaking surface waves in shallow water, *J. Geophys. Res.*, *102*, 25,035–25,046, 1997.

Eckart, C., Surface waves on water of variable depth, *Wave Rep. 100*, 99 pp., Scripps Inst. of Oceanogr., Univ. of California, La Jolla, Calif., 1951.

Eldeberky, Y., and J. A. Battjes, Spectral modeling of wave breaking: Application to Boussinesq equations, *J. Geophys. Res.*, *101*, 1253–1264, 1996.

Elgar, S., and R. T. Guza, Observations of bispectra of shoaling surface gravity waves, *J. Fluid Mech.*, *161*, 425–448, 1985.

Elgar, S., R. T. Guza, and M. H. Freilich, Observations of nonlinear interactions in directionally spread shoaling surface gravity waves, *J. Geophys. Res.*, *98*, 20,299–20,305, 1993.

Elgar, S., T. H. C. Herbers, and R. T. Guza, Reflection of ocean surface gravity waves from a natural beach, *J. Phys. Oceanogr.*, *24*, 1503–1511, 1994.

Elgar, S., R. T. Guza, B. Raubenheimer, T. H. C. Herbers, and E. L. Gallagher, Spectral evolution of shoaling and breaking waves on a barred beach, *J. Geophys. Res.*, *102*, 15,797–15,805, 1997.

Elgar, S., R. T. Guza, W. C. O'Reilly, B. Raubenheimer, and T. H. C. Herbers, Wave energy and direction observed near a pier, *J. Waterw. Port Coastal Ocean Eng.*, *127*, 2–6, 2001.

Feddersen, F., R. T. Guza, S. Elgar, and T. H. C. Herbers, Alongshore momentum balances in the nearshore, *J. Geophys. Res.*, *103*, 15,667–15,676, 1998.

Freilich, M. H., and R. T. Guza, Nonlinear effects on shoaling surface gravity waves, *Philos. Trans. R. Soc. London, Ser. A*, *311*, 1–41, 1984.

Freilich, M. H., R. T. Guza, and S. Elgar, Observations of nonlinear effects in directional spectra of shoaling gravity waves, *J. Geophys. Res.*, *95*, 9645–9656, 1990.

Gallagher, E. L., S. Elgar, and R. T. Guza, Observations of sand bar evolution on a natural beach, *J. Geophys. Res.*, *103*, 3203–3215, 1998.

Hasselmann, K., On the non-linear energy transfer in a gravity-wave spectrum, 1, General theory, *J. Fluid Mech.*, *12*, 481–500, 1962.

Herbers, T. H. C., and R. T. Guza, Estimation of directional wave spectra from multicomponent observations, *J. Phys. Oceanogr.*, *20*, 1703–1724, 1990.

Herbers, T. H. C., and M. C. Burton, Nonlinear shoaling of directionally spread waves on a beach, *J. Geophys. Res.*, *102*, 21,101–21,114, 1997.

Herbers, T. H. C., R. L. Lowe, and R. T. Guza, Field observations of orbital velocities and pressure in weakly nonlinear surface gravity waves, *J. Fluid Mech.*, *245*, 413–435, 1992.

Herbers, T. H. C., S. Elgar, and R. T. Guza, Directional spreading of waves in the nearshore, *J. Geophys. Res.*, *104*, 7683–7693, 1999.

Herbers, T. H. C., N. R. Russnogle, and S. Elgar, Spectral energy balance of breaking waves within the surf zone, *J. Phys. Oceanogr.*, *30*, 2723–2737, 2000.

Holloway, G., and M. C. Hendershott, Stochastic closure for nonlinear Rossby waves, *J. Fluid Mech.*, *82*, 747–765, 1977.

Kaihatu, J. M., and J. T. Kirby, Nonlinear transformation of waves in finite water depth, *Phys. Fluids*, *7*, 1903–1914, 1995.

Lamb, H., *Hydrodynamics*, 6th ed., 738 pp., Cambridge Univ. Press, New York, 1932.

Mase, H., and J. T. Kirby, Hybrid frequency-domain KdV equation for random wave transformation, in *Proceedings of the 23rd International Conference on Coastal Engineering*, pp. 474–487, Am. Soc. of Civ. Eng., New York, 1992.

Norheim, C. A., T. H. C. Herbers, and S. Elgar, Nonlinear evolution of surface wave spectra on a beach, *J. Phys. Oceanogr.*, *28*, 1534–1551, 1998.

Orszag, S. A., Analytical theories of turbulence, *J. Fluid Mech.*, *41*, 363–386, 1970.

Peregrine, D. H., Long waves on a beach, *J. Fluid Mech.*, *27*, 815–827, 1967.

Phillips, O. M., On the dynamics of unsteady gravity waves of finite amplitude, 1, The elementary interactions, *J. Fluid Mech.*, *9*, 193–217, 1960.

Schäffer, H. A., P. A. Madsen, and R. Deigaard, A Boussinesq model for wave breaking in shallow water, *Coastal Eng.*, *20*, 185–202, 1993.

Thornton, E. B., and R. T. Guza, Transformation of wave height distribution, *J. Geophys. Res.*, *88*, 5925–5938, 1983.

Ursell, F., Edge waves on a sloping beach, *Proc. R. Soc. London, Ser. A*, *214*, 79–97, 1952.

WAMDI GROUP, The WAM Model-A Third Generation Ocean Wave Prediction Model, *J. Phys. Oceanogr.*, *18*, 1775–1810, 1988.

Wei, G., J. T. Kirby, S. T. Grilli, and R. Subramanya, A fully nonlinear Boussinesq model for surface waves, 1, Highly nonlinear unsteady waves, *J. Fluid Mech.*, *294*, 71–92, 1995.

Whitford, D. J., Wind and wave forcing of longshore currents across a barred beach, Ph.D. thesis, Nav. Postgraduate Sch., Monterey, Calif., 1988.

S. Elgar, Department of Applied Ocean Physics and Engineering MS#11, Woods Hole Oceanographic Institution, Woods Hole, MA 02543, USA. (selgar@whoi.edu)

R. T. Guza, Integrative Oceanography Division, Scripps Institution of Oceanography, La Jolla, CA 92093-0209, USA. (rtg@coast.ucsd.edu)

T. H. C. Herbers and M. Orzech, Department of Oceanography, Naval Postgraduate School, Monterey, CA 93943-5122, USA. (thherber@nps.navy.mil; orzech@nps.navy.mil)